Scripta Materialia 190 (2021) 147–152

Contents lists available at ScienceDirect

Scripta Materialia

journal homepage: www.elsevier.com/locate/scriptamat

Deformation state extraction from electron backscatter diffraction patterns via simulation-based pattern-matching

Christian Kurniawan, Chaoyi Zhu, Marc DeGraef*

Department of Material Science and Engineering, Carnegie Mellon University, Pittsburgh, PA 15213, USA

ARTICLE INFO

Article history:
Received 1 May 2020
Revised 2 September 2020
Accepted 3 September 2020
Available online 9 September 2020

Keywords:
Plastic deformation
Electron backscatter diffraction (EBSD)
Simulation
Dislocation
Deformation state extraction
Pattern-matching

ABSTRACT

A new simulation-based pattern-matching method is developed to retrieve the deformation tensor from electron backscatter diffraction patterns. Minimizing the least-squares difference between a target pattern and simulated deformed patterns, the deformation state of the target pattern can be inferred with an average absolute error of $\sim 10^{-8}$ for the distortion tensor under ideal conditions. The new approach is robust against significant pattern rotation compared to the cross-correlation based method. Additionally, the pattern center can be simultaneously optimized with an average absolute distortion tensor error of $\sim 10^{-4}$ for noise-free patterns.

With the rapid development of automated electron backscatter diffraction (EBSD) [1,2], the technique has become a popular tool to characterize location-specific crystallographic orientation and deformation information [3]. In the area of deformation studies, the determination of the deformation tensor from the EBSD pattern (EBSP), a technique widely known as the high angular resolution EBSD (HR-EBSD) method [4–6], has been particularly successful. Additional studies have refined this method by applying a remapping method to compensate for the phantom strain associated with large pattern rotations [7–9] or a more global approach to deformation extraction [10–12]. These global approaches in principle utilize the same crystal deformation framework to relate differences in the diffraction patterns (shifts of the whole pattern and changes in the inter-planar angles in Kikuchi bands) to uniquely solve for the corresponding deformation tensor. The HR-EBSD method is reported to achieve an average absolute error of $\sim 10^{-4}$ for rotation and strain tensor components [5]. However, the requirement for a deformation-free (or known deformation state) reference pattern can prove to be a major limitation. Simulation-based HR-EBSD methods have been proposed to determine the deformation state of an experimental pattern by cross-correlating it with a simulated undeformed reference pattern [7,13–15]. The deformed (i.e., elastically strained) test pattern is typically simulated by adjusting the lattice parameters to recompute the deformed pattern. The most common concern for the use of simulation-based HR-EBSD is related to the uncertainties in the simulation parameters that could degrade the accuracy of the approach [16–21]. More recently, several research groups have developed pattern-matching methods to determine tetragonality in martensite [22], refine the orientation [23–26] and the pattern center (PC) [15,27,28] analysis. However, the direct determination of the deformation tensor via a whole pattern-matching approach has yet to be developed and is addressed here.

In this study, we demonstrate the possibility of direct inference of the deformation tensor via a simulation-based whole pattern matching approach. By comparing the target pattern with simulated deformed patterns generated on the fly, we can directly infer the deformation tensor. Since the physical model for the crystal deformation has already been accounted for in the simulation of the deformation diffraction pattern, the problem of deformation tensor inference essentially becomes a multiparameter optimization problem in search of the combination of deformation tensor and pattern center which produces the best match to the target pattern. This is in direct contrast to the feature extraction approach used by many global registration papers in which they must rigorously formulate shifts in the diffraction pattern to obtain the deformation tensor [12,29]. To evaluate the performance of our method, we compare it with the conventional cross-correlation based HR-EBSD method. In this preliminary research, we consider an ideal case in which all the deformed patterns, including the background intensity obtained from Monte Carlo simulation, are simulated using the EMsoft open-source package [30]. More realistic considerations such as noise, the effect of binning, and pattern center

* Corresponding author.
E-mail address: mdg@andrew.cmu.edu (M. DeGraef).

https://doi.org/10.1016/j.scriptamat.2020.09.004

uncertainty are also assessed. This paper is organized as follows: first, we outline the simulation technique to obtain deformed EBSPs and the computation of the surface deformation field around a single edge dislocation; then we describe the method used to infer the deformation; we conclude with a comparison of our approach with the cross-correlation based HR-EBSD method.

The simulation of EBSPs in the current study merges Bloch-wave based dynamical electron-scattering computations with the Monte-Carlo simulation of energy, depth, and directional distributions of the backscattered electrons (BSEs) [31,32]. First, the master pattern is generated and stored as a square Lambert projection, which is an equal-area mapping of a unit hemisphere of the Kikuchi sphere. The EMsoft package was used to generate the undistorted master pattern of cubic-crystal Nickel with a 0.35236 nm lattice parameter and Debye-Waller factor equal to 0.0035 nm^2. The following Monte Carlo parameters were used: 2×10^9 total number of electrons; 70° sample tilt angle from horizontal; 20 keV incident beam energy with 10 keV minimum energy to consider and 1 keV energy bin size; 100 nm maximum depth with 1 nm step size. The package generated the master pattern of size 1001 × 1001 pixels with 0.05 nm as the smallest d-spacing. For a given crystal orientation and detector geometry, the EBSP can then be extracted from the master pattern through an interpolation exercise (detailed mathematical formulation can be found in the supplementary material).

In principle, deformed master patterns can be generated by evaluating the backscattering yield for a deformed crystal based on the displaced lattice positions. However, this can be a computationally demanding task to recompute every distorted master pattern in the strain space. Alternatively, the deformation tensor can be approximately imposed by modifying the position vectors of the detector pixels by the inverse of the deformation tensor, with respect to the sample reference frame, to the undistorted master pattern during the interpolation step for each EBSP simulation.[1] The EMEBSD program in the EMsoft package [30] was adapted with this additional transformation, and used to obtain distorted EBSPs for the following experimental parameters: 10° camera tilt angle; 150 nA incident beam current with 100 µs dwell time; 0.333 gamma value for intensity scaling. The pattern size was set to 1000 × 1000 pixels with no binning and an individual (square) pixel size 50µs. Initially, we set the pattern center (x_{pc}, y_{pc}) at the center of the detector with a scintillator-sample distance (L) of 25,000µs. An example simulated pattern for Euler angles $(\varphi_1, \Phi, \varphi_2) = (0, 0, 0)$ is shown in Fig. 1(b). The energy distribution for BSEs simulated at 20 keV will also have higher energy electrons scattered close to the bottom of the scintillator, similar to the case of 30 keV on Ni. The weighting of the dynamic scattering simulation by the energy histogram of the Monte Carlo data is carried out according to equations 12 and 13 in Callahan and Graef [31].

For the deformation state, we employed an analytical expression of the deformation tensor field around a single surface-penetrating edge dislocation in Nickel using the (elastically isotropic) Yoffe-Shaibani-Hazzeldine (YSH) model [33,34]; this deformation state is considered to be the ground truth for our simulations and comparisons. The YSH model utilizes an image dislocation to guarantee the traction free boundary condition on a semi-infinite surface, which applies to an actual EBSD measurement [35]. With the YSH model, we first obtained the analytical solution for the displacement field as a function of three spatial coordinates for a given configuration of dislocation. The [1 0 0] Burgers vector of the edge dislocation runs along the horizontal direction (see Fig. 1(a)), placing the extra half-plane in the top half of the region. The displacement gradients were computed analytically and used to populate the displacement gradient portion of the distortion tensor. By putting the spatial coordinates into the analytical solution of the distortion tensor field, we generated an array of size 51 × 51 of free surface deformation gradient tensors (distortion tensor plus the identity matrix) with a step size of 3 nm. Note that the full deformation data set was three-dimensional and only the free surface solution was used here as the input deformation gradient tensor field. For verification, we have checked that the surface stress is all zero ($\sigma_{i3} = 0, i = 1, 2, 3$) and the YSH model converges to the infinite medium solution of the distortion field of an edge dislocation at $-\infty$. However, the use of the analytical dislocation data set does not consider realistic interaction volume. Therefore, the accuracy claimed below serves as a way of verifying the method we have proposed here, which does not directly reflect real-world dislocation mapping.

Since the hydrostatic dilatation does not change the crystallographic directions projected onto the phosphor screen [5,35], there are effectively only eight, instead of nine, degrees of freedom. Therefore, additional constraints must be imposed to determine the hydrostatic part of the deformation, which can be done by applying either the full ($\sigma_{i3} = 0, i = 1, 2, 3$) or partial ($\sigma_{33} = 0$) traction free boundary condition. In this study, we applied the constraint $\sigma_{33} = 0$ to obtain the final degree of freedom after the other eight degrees of freedom had been fully determined with our optimization approach. Following the generalized Hooke's law, this constraint can be reformulated as:

$$C_{33}\epsilon_{33} + C_{12}(\epsilon_{11} + \epsilon_{22}) = \sigma_{33} = 0 \tag{1}$$

where C_{33}, C_{12} are the components of the stiffness matrix of the test material (Nickel). Since $\epsilon_{11} - \epsilon_{33}$ and $\epsilon_{22} - \epsilon_{33}$ can be determined from the distortion tensor ($\boldsymbol{\beta}$), ϵ_{33} can be determined uniquely from Eq. (1) through appropriate substitution. For experimental data, the stiffness tensor components are sensitive to the alloying elements, which could contribute to potential bias in the constraint. It does not constitute as a concern since the stiffness values are identical in the YSH model and the traction free boundary condition.

The EMEBSD program used to compute the patterns can be thought of as the forward model for obtaining the individual pixel intensities of an EBSP ($\mathbf{I}_{\text{EBSP}}$), for a given β' representing the vector containing the eight degrees of freedom of the distortion tensor β. Theoretically, we can then solve this forward model for β' to extract the deformation tensor from the EBSP. However, for EBSP obtained experimentally, which will be the real-world scenario, the forward model is at best an approximation of reality, and its exact form is unknown; thus, an analytical solution for β' becomes impractical. A more direct approach, similar to the method used in Winkelmann et al. [22], 26], Pang et al. [36], is to minimize the error between the obtained $\mathbf{I}_{\text{EBSP}}$ and the predicted pixel intensity ($\mathbf{I}_{\text{pred.}}$) over the domain $\mathcal{D}$ of β'. The solution of the problem can then be stated in the form of a minimization problem:

$$\beta' \approx \text{argmin}_{\beta'_{\text{pred.}}} E(\beta'_{pred.}) \quad \text{with} \quad \beta'_{\text{pred.}} \in \mathcal{D}(\beta') \tag{2}$$

where $E(\beta'_{\text{pred.}})$ quantifies the error between $\mathbf{I}_{\text{EBSP}}$ and $\mathbf{I}_{\text{pred.}}$. The simplest choice for the error measurement is the sum of the squared difference over all pixels of the whole pattern:

$$E(\beta'_{pred.}) = \sum_{j=1}^{n} (i_j - i_j^*)^2, \tag{3}$$

[1] Our approximation method does not account for the changes in Bragg angles due to the deformation. However, we choose to ignore this because the changes are small for small strains, and, to first order, they only affect the width of the Kikuchi bands as well as the positions of higher-order diffraction features while the geometry of the deformation, including the positions of the zone axes and band center lines, are correctly accounted for.

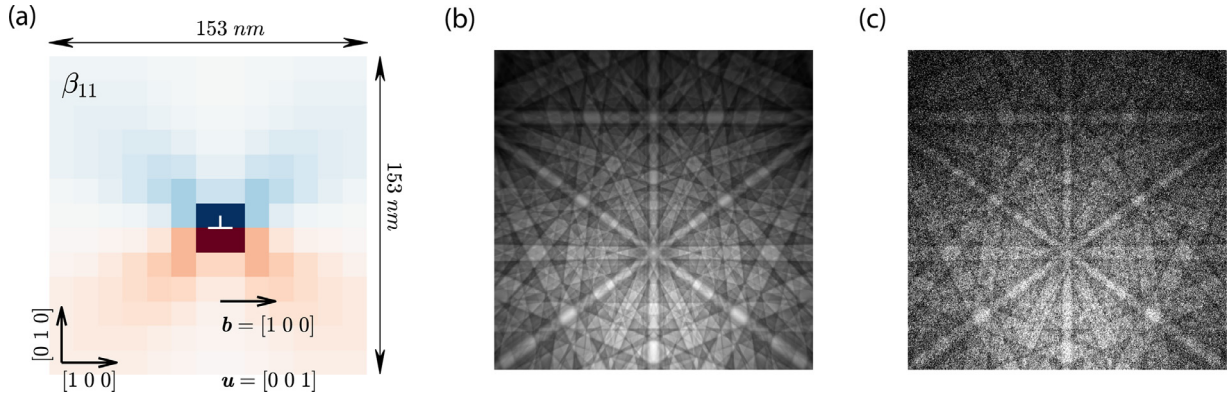

Fig. 1. **(a)** is a schematic of the dislocation geometry. **(b)** is a strain-free EBSP of Nickel, generated using the EMEBSD program in the EMsoft package [30]; simulation parameters are listed in the text. **(c)** is a strain-free EBSP of Nickel with peak signal-to-noise ratio of ~ 14.7 dB introduced.

for $\mathbf{I}_{\text{EBSP}} = \{i_1, i_2, \ldots, i_n\}$ where i_j is the intensity of the jth pixel (n is the total number of pixels in a pattern) and $\mathbf{I}_{\text{pred.}} = \{i_1^*, i_2^*, \ldots, i_n^*\}$.

Because the function $E(\beta'_{pred.})$ does not necessarily have a smooth landscape in all directions, we utilized the particle swarm optimization (PSO) algorithm [37] with 100 population size and ran it until 75% rate of convergence or 20 iterations is reached. We then employed the Nelder-Mead Simplex algorithm [38], as implemented in Matlab's `fminsearchbnd()` function [39] to refine the solution. We set −0.03 and 0.03 as the lower and upper bounds for the optimization scheme, which is about ten times larger than the distortion tensor elements of our test data (i.e., $[-0.0027, 0.0027]$) and much larger than the elastic limit of most metals, i.e. 0.002. The initial population of the optimization was generated from a normal distribution around the origin with a standard deviation equal to one-fourth of the upper bound.

We compared the performance of our approach with the widely used cross-correlation based HR-EBSD method. We extracted the distortion tensor components from the array of simulated EBSPs using both cross-correlation based HR-EBSD and our pattern-matching method. In this comparison, we implemented the cross-correlation based HR-EBSD approach with a first pass cross-correlation based remapping, modified from a code developed by Zhu et al. [9] with necessary adaptation to address the traction free boundary condition. The plots representing the actual distortion with its inferences and the absolute error of the two methods are displayed in Fig. 2. The average absolute errors are $\sim 3.2 \times 10^{-8}$ and $\sim 1.2 \times 10^{-5}$ for the pattern-matching and cross-correlation based HR-EBSD methods, respectively. Hence, the pattern-matching method has an overall lower error compared to the cross-correlation based HR-EBSD method, suggesting that our approach provides a promising new direction in deformation tensor extraction.

A quantitative comparison between both methods is shown in the box-plots of Fig. 3; in **(a)**, we compare the absolute error for both approaches as a function of the magnitude of the rotational part of the deformation tensor[2] (by multiplication of the original rotational part by integral factors). We adjusted the size of the search domain for β' by the same multiplicative factor. The box-plots in Fig. 3**(a)** show that the new method still surpasses the cross-correlation approach even with an increased rotational part.

We also inspected the possibility of applying the new approach for binned pattern data sets. We effectively lowered the pattern resolution by increasing the binning during the simulation process. The comparison of the absolute error for both HR-EBSD and pattern-matching methods to recover distortion tensors from various binning can be seen in Fig. 3**(b)**. Overall, the pattern-matching approach still outperforms the cross-correlation based HR-EBSD method as pattern resolution is binned to 125 × 125 pixels because the current binning introduced still over-samples the intensity information such as orientation and deformation. Based on this, the new approach could be a more feasible direction to recover deformation tensor for binned patterns to obtain similar accuracy as the available cross-correlation HR-EBSD, which reduces scan acquisition time.

With the introduction of noise, a higher error would be expected [5,40]. To investigate this, we introduced Gaussian noise in the deformed patterns, generated using `imnoise()` operator available in Matlab's image processing toolbox with variances of 0.001, 0.01, 0.02, 0.04, and 0.1, which correspond to an approximate peak signal-to-noise ratio of 30, 20.2, 17.4, 14.7, and 11.5 dB, respectively. The updated average absolute error in Fig. 3**(c)** indicates that our approach is more sensitive to the pattern noise but start to converge at peak signal-to-noise ratio of ~ 14.7 dB (an undistorted pattern with this level of noise can be seen in Fig. 1(c)). Furthermore, the pattern-matching method does appear to have a more stable accuracy of $\sim 4 \times 10^{-4}$ average absolute error while the cross-correlation's performance decreases gradually in extracting the deformation tensor from patterns with peak signal-to-noise ratio of ~ 14.7 dB in increasing rotational component (see Fig. 3**(d)**). The comparison reveals that our approach might reduce the problem of phantom strain commonly associated with cross-correlation based technique.

Lastly, we tested the robustness of the new method against experimental uncertainties, such as pattern center inaccuracy. We modified Eq. (2) such that an additional three degrees of freedom for the pattern center (x_{pc}, y_{pc}, L) were simultaneously considered. This allowed us to infer PC in addition to β', for a total of 11 degrees of freedom. We then applied the same optimization process with the initial population for the PC was generated from a normal distribution around the actual value with a standard deviation equal to 0.25% of the pattern width, which is a realistic PC error [18]. To ease the optimization scheme, we rescaled L into pixel units by dividing the pixel size (i.e. 50 μm) into L then shifted it by half of the pattern width so that the domain of L is equal to the domain of x_{pc} and y_{pc}. During the optimization, we also rescaled PC by 1% of the pattern width, which is the absolute bounds we chose for the PC, and divided it by the upper bound of the distortion domain so that both PC and distortion has the same domain. To provide an estimated accuracy of the method under experimental data, we also performed the procedure for patterns with a peak

[2] Note that deformation tensor has both a rotational and a strain component which can be extracted by means of polar decomposition.

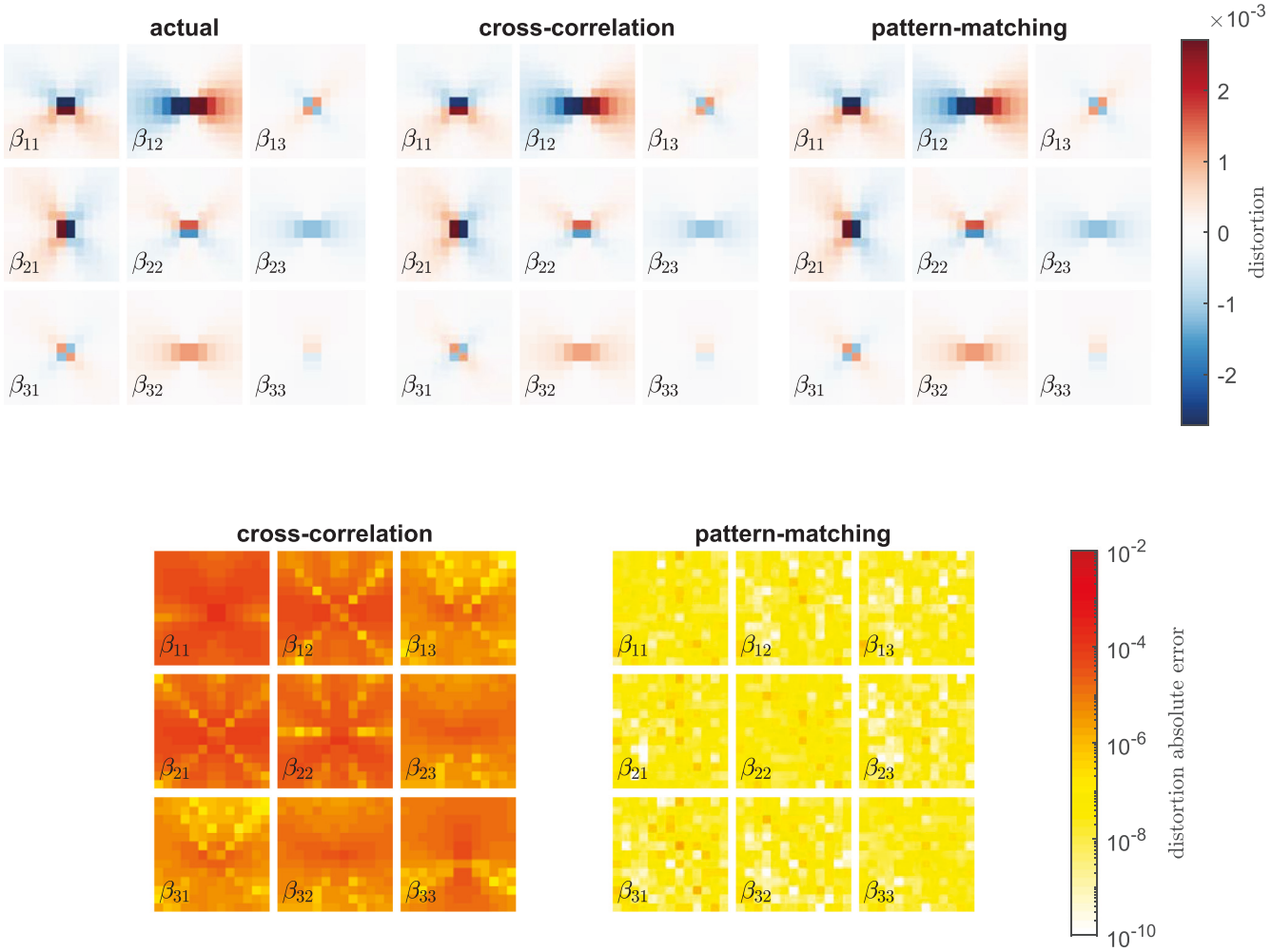

Fig. 2. Contour plots for each element of the three by three matrices representing the value of the actual and inferred distortion tensors **(top)** with its absolute error **(bottom)**. Both pattern center and orientation are treated as known quantities in the optimization. The distortion tensor inference was carried out using both the cross-correlation based and the pattern-matching HR-EBSD methods.

signal-to-noise ratio of ~ 14.7 dB. The box-plot representing the error of the inferred pattern center as a fraction of the percent of pattern width can be seen in Fig. 4**a**, which provides a comparable result to that presented in Pang et al. [36]. Fig. 4**(b)** shows the distortion absolute error comparison of the new approach with uncertain PC which clearly shows compromised accuracy. While the accuracy of the distortion is acceptable in the case of noise-free pattern $\sim \times 10^{-4}$, the current state of our approach will only achieve an accuracy of $\sim 10^{-3}$ when taking into account of both pattern center inaccuracy and a significant amount of noise. Hence, high-quality patterns obtained under long exposure or appropriate pattern filtering are needed for the current method to achieve a more desirable accuracy.

We also note here that the new approach has not yet been tested on experimental data, thus the claimed accuracy value may not be representative of that achievable on experimental data. For experimental patterns, an appropriate method for back-correction is required to adjust the brightness and contrast of patterns to avoid biases introduced in the residual errors. Moreover, lens distortion needs to be corrected for experimental patterns prior to the application of the forward model-based pattern matching approach to reduce potential systematic error. Additionally, the new approach requires significantly more computational time, ~ 20 min/result, than the HR-EBSD approach, ~ 0.5 min/result (executed under the same MATLAB environment on the same machine). The accuracy and time limitation of the method might be improved by replacing the optimization scheme using a faster and more robust optimization algorithm. Alternatively, selection of a different $E(\beta'_{\text{pred.}})$ function with a smoother and more prominent slope may also enhance the speed and accuracy of the new method. This approach can be thought of as a simplified version of the inverse problem theory [41–44]; thus, incorporating a probability density function (PDF) to represent the simulation uncertainties, e.g., for the PC uncertainty, may offer a path to applying the new approach for real data sets. A further comparison between experimental and simulation data will be needed to determine the appropriate type of PDF to be introduced. We also see the opportunity here to complement the HR-EBSD method with the whole-pattern matching approach, specifically for the reference patterns used in HR-EBSD, as a means towards the ultimate goal of 'absolute' strain mapping with EBSD technique.

In summary, we have introduced a new approach for deformation state extraction from EBSPs via the whole pattern-matching by minimizing the intensity differences of the target and simulated patterns. We compared the method's performance to the conventional cross-correlation HR-EBSD method and showed that under ideal conditions (no noise with exact knowledge of pattern center), the new approach outperforms the HR-EBSD method. In addition, we demonstrated that the new method is more robust for patterns with significant rotation, reducing the problem of phantom strain.

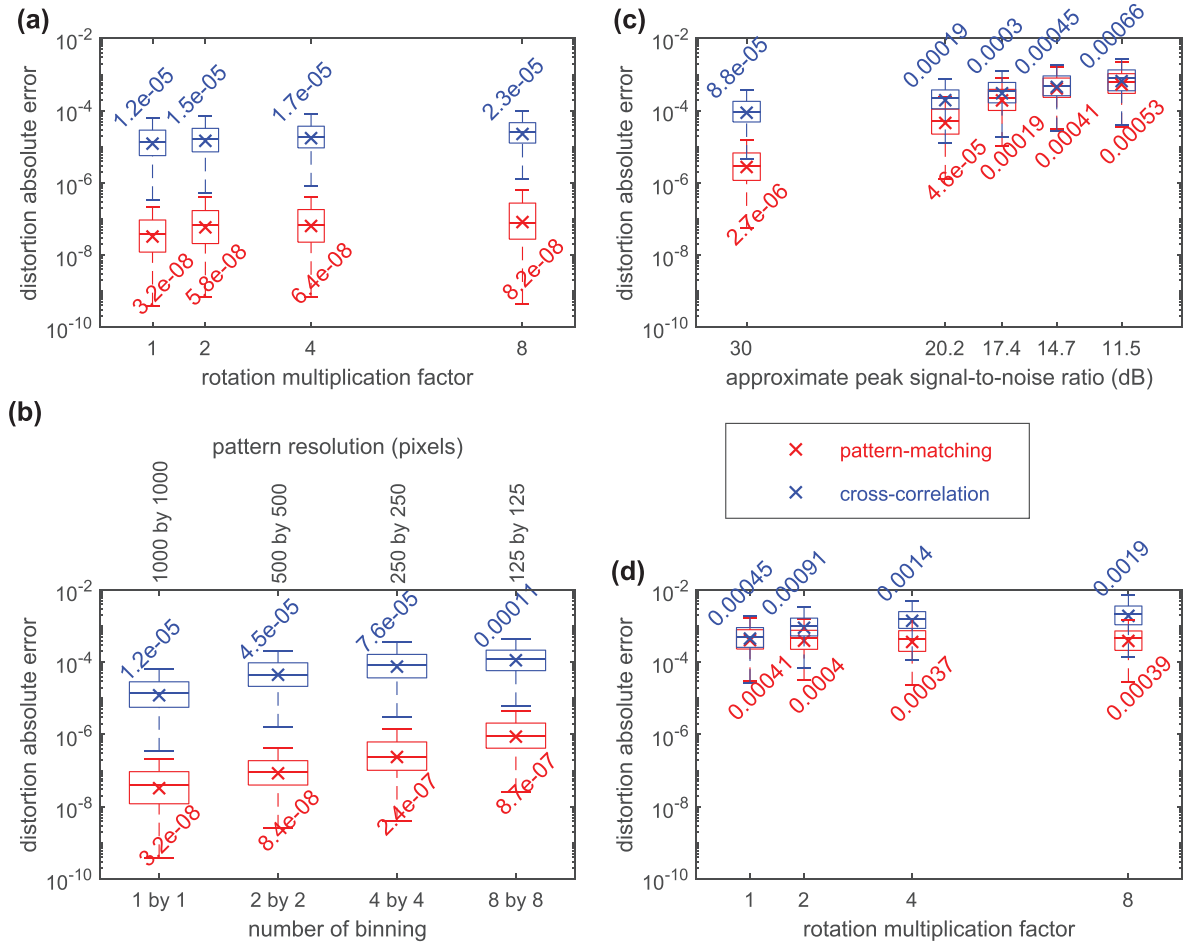

Fig. 3. Box-plots comparing the absolute error of the deformation extraction via the cross-correlation based and the pattern-matching HR-EBSD where the × markers show the average absolute error of both approaches (values are displayed). Both pattern center and orientation are treated as known quantities in the optimization. **(a)** shows the absolute error as a function of increasing rotational component. **(d)** shows the absolute error with different binning or pattern resolutions. **(c)** shows the absolute error from patterns with increasing noise. **(d)** shows the absolute error from patterns with peak signal-to-noise ratio of ~ 14.7 dB in increasing rotation cases.

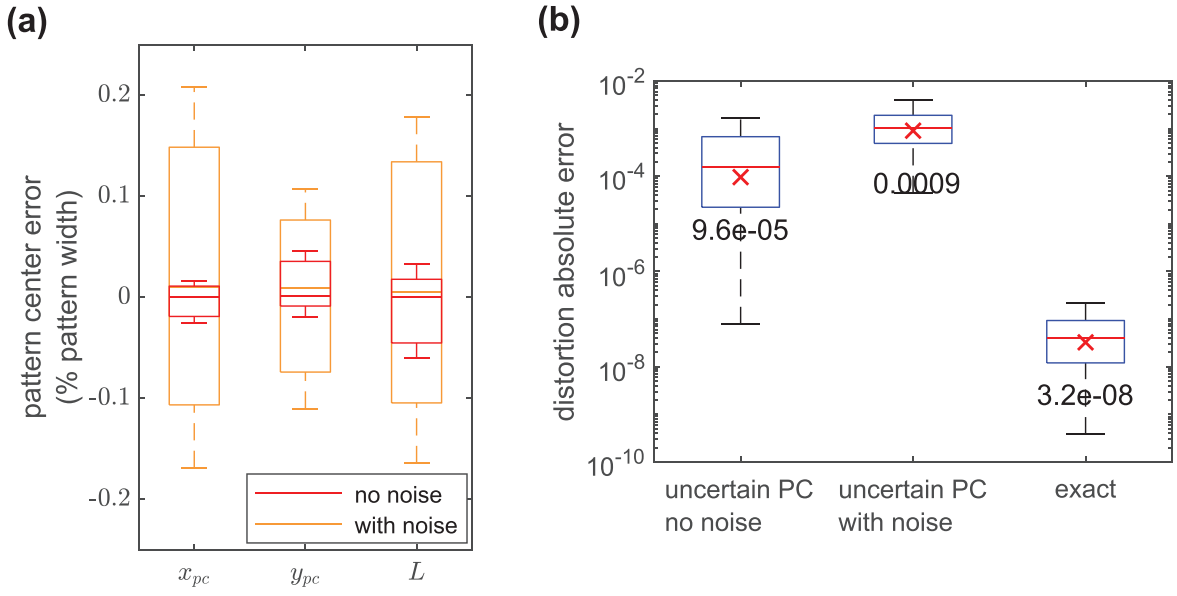

Fig. 4. Simultaneous inference of pattern center and deformation tensor. **(a)** shows the box-plot of pattern center error extracted from patterns with both noise-free and ~ 14.7 peak signal-to-noise ratio. **(b)** shows the box-plot of distortion absolute error obtained using the pattern-matching approach for uncertain pattern center from patterns with zero noise and peak signal-to-noise ratio of ~ 14.7 dB. × markers shows the average absolute error for the two cases (values are displayed) and the exact case is displayed as the control.

Lastly, the new approach can retrieve the deformation tensor for binned patterns. We see three feasible paths for improvements to the approach: improving the optimization step using a faster and more robust optimization algorithm; implementing noise filters to improve pattern quality; and selecting a model with a smoother surface and more prominent slope, and/or incorporating a probability density function (PDF) to represent simulation uncertainty.

Declaration of Competing Interest

None.

Acknowledgments

The material presented here is based upon work supported by the National Science Foundation under grant no. DMR-1904629. We would like to show our gratitude for the insights from Dr. W. Lenthe, Dr. E. Pascal, Z. Ding, M. Kitcher, N. Pandei, J. Tessmer, K.-W. Jin, M. Li, and M. Ochsendorf during the course of this research. We also acknowledge the use of the computational resources of the Materials Characterization Facility at Carnegie Mellon University supported by grant MCF-677785.

Supplementary material

Supplementary material associated with this article can be found, in the online version, at 10.1016/j.scriptamat.2020.09.004

References

[1] S.I. Wright, B.L. Adams, Metall. Trans. A 23 (1992) 759–767.
[2] N.C.K. Lassen, Scanning Microsc. 6 (1992) 115–121.
[3] A.J. Schwartz, M. Kumar, B.L. Adams (Eds.), Electron Backscatter Diffraction in Material Science, Springer Science & Business Media, 2000.
[4] K.Z. Troost, P.V.D. Sluis, D.J. Gravesteijn, Appl. Phys. Lett. 62 (1993) 1110–1112.
[5] A.J. Wilkinson, G. Meaden, D.J. Dingley, Ultramicroscopy 106 (2006) 307–313.
[6] S. Villert, C. Maurice, C. Wyon, R. Fortunier, J. Microsc. 233 (2009) 290–301.
[7] T.B. Britton, A.J. Wilkinson, Ultramicroscopy 114 (2012) 82–95.
[8] C. Maurice, J.H. Driver, R. Fortunier, Ultramicroscopy 113 (2012) 171–181.
[9] C. Zhu, K. Kaufmann, K.S. Vecchio, Ultramicroscopy 208 (2020) 112851.
[10] C. Maurice, E. Plancher, H. Klocker, Poster session of RMS EBSD meeting, https://www.researchgate.net/publication/314095375_A_novel_finite_strain_framework_for_HR-EBSD. 10.13140/RG.2.2.33748.81282,
[11] T. Vermeij, J.P. Hoefnagels, Ultramicroscopy 191 (2018) 44–50.
[12] C. Ernould, B. Beausir, J.J. Fundenberger, V. Taupin, E. Bouzy, Acta Mater. 191 (2020) 131–148, doi:10.1016/j.actamat.2020.03.026.
[13] J. Kacher, C. Landon, B.L. Adams, D. Fullwood, Ultramicroscopy 109 (2009) 1148–1156.
[14] D. Fullwood, M. Vaudin, C. Daniels, T. Ruggles, S.I. Wright, Mater. Charact. 107 (2015) 270–277.
[15] T. Tanaka, A.J. Wilkinson, Ultramicroscopy 202 (2019) 87–99.
[16] C. Maurice, R. Fortunier, J. Driver, A. Day, K. Mingard, G. Meaden, Ultramicroscopy 110 (2010) 758–759.
[17] J. Kacher, J. Basinger, B.L. Adams, D.T. Fullwood, Ultramicroscopy 110 (2010) 760–762.
[18] T.B. Britton, C. Maurice, R. Fortunier, J.H. Driver, A.P. Day, G. Meaden, D.J. Dingley, K. Mingard, A.J. Wilkinson, Ultramicroscopy 110 (2010) 1443–1453.
[19] K. Mingard, A. Day, C. Maurice, P. Quested, Ultramicroscopy 111 (2011) 320–329.
[20] J. Alkorta, Ultramicroscopy 131 (2013) 33–38.
[21] J. Alkorta, M. Marteleur, P.J. Jacques, Ultramicroscopy 182 (2017) 17–27.
[22] A. Winkelmann, G. Nolze, G. Cios, T. Tokarski, Phys. Rev. Mater. 2 (2018) 1–15, doi:10.1103/PhysRevMaterials.2.123803.
[23] Y.H. Chen, S.U. Park, D. Wei, G. Newstadt, M.A. Jackson, J.P. Simmons, M. De Graef, A.O. Hero, Microsc. Microanal. 21 (2015) 739–752.
[24] A.J. Wilkinson, D.M. Collins, Y. Zayachuk, R. Korla, A. Vilalta-Clemente, Ultramicroscopy 196 (2019) 88–98.
[25] A. Foden, D.M. Collins, A.J. Wilkinson, T.B. Britton, Ultramicroscopy 207 (2019) 112845.
[26] A. Winkelmann, B.M. Jablon, V.S. Tong, C. Trager-Cowan, K.P. Mingard, J. Microsc. 277 (2020) 79–92, doi:10.1111/jmi.12870.
[27] G. Nolze, M. Jürgens, J. Olbricht, A. Winkelmann, Acta Mater. 159 (2018) 408–415.
[28] T. Friedrich, A. Bochmann, J. Dinger, S. Teichert, Ultramicroscopy 184 (2018) 44–51.
[29] C. Ernould, B. Beausir, J.-J. Fundenberger, V. Taupin, E. Bouzy, Scr. Mater. 185 (2020) 30–35.
[30] M.D. Graef, M. Jackson, J. Kleingers, C. Zhu, josephtessmer, wlenthe, saransh13, M. Atkinson, S. Wright, H. Ånes, EMsoft-org/EMsoft: EMsoft Release 5.0.0, 2019.
[31] P.G. Callahan, M.D. Graef, Microsc. Microanal. 19 (2013) 1255–1265.
[32] C. Zhu, M. De Graef, Ultramicroscopy 218 (2020) 113088, doi:10.1016/j.ultramic.2020.113088. URL: https://linkinghub.elsevier.com/retrieve/pii/S0304399120302394
[33] S.J. Shaibani, P.M. Hazzledine, Philos. Mag. A 44 (1981) 657–665.
[34] E.H. Yoffe, Philos. Mag. 6 (1961) 1147–1155.
[35] T.J. Hardin, T.J. Ruggles, D.P. Koch, S.R. Niezgoda, D.T. Fullwood, E.R. Homer, J. Microsc. 260 (2015) 73–85.
[36] E.L. Pang, P.M. Larsen, C.A. Schuh, Ultramicroscopy 209 (2019) 112876.
[37] J. Kennedy, R. Eberhart, Particle swarm optimization, Proceedings of ICNN'95 - International Conference on Neural Networks, vol. 4, Perth, WA, Australia, 1995, pp. 1942–1948, doi:10.1109/ICNN.1995.488968.
[38] J.A. Nelder, R. Mead, Comput. J. 7 (1965) 308–313.
[39] J. D'Erico, fminsearchbnd v.1.4, bound constrained optimization using fminsearch, 2012.
[40] A.J. Wilkinson, G. Meaden, D.J. Dingley, Mater. Sci. Technol. 22 (2006) 1271–1278.
[41] A. Tarantola, B. Valette, Rev. Geophys. Space Phys. 20 (1982) 219–232.
[42] A. Tarantola, B. Valette, J. Geophys. 50 (1982) 159–170.
[43] K. Mosegaard, A. Tarantola, International Handbook of Earthquake & Engineering Seismology (Part A), Academic Press, 2002, pp. 237–265.
[44] A. Tarantola, Inverse Problem Theory and Methods for Model Parameter Estimation, Society for Industrial and Applied Mathematics, Philadelphia, 2005.